

Microstructure-based Stress Modeling of Tin Whisker Growth

Jie-Hua Zhao, Peng Su, Min Ding, Sheila Chopin, and Paul S. Ho

Abstract

A 3-dimensional finite element method (FEM) model considering the elasticity anisotropy, thermal expansion anisotropy and plasticity of β -Sn is established. The Voronoi diagrams are used to generate the geometric patterns of grains of the Sn coating on Cu leadframes. The crystal orientations are assigned to the Sn grains in the model using the x-ray diffraction (XRD) measurement data of the samples. The model is applied to the Sn-plated package leads under thermal cycling tests. The strain energy density (SED) is calculated for each grain. It is observed that the samples with higher calculated SED are more likely to have longer Sn whiskers and higher whisker density. The FEM model, combined with the XRD measurement of the Sn finish, can be used as an effective indicator of the Sn whisker propensity. This may expedite the qualification process significantly.

Index Terms

Sn whisker, Tin whisker, Pb-free, leadfree, package, stress, strain energy density, Voronoi diagram, x-ray diffraction, finite element method

I. INTRODUCTION

THE global movement towards Pb-free electronic products has posed many challenges to the research and development of electronic packaging. One example is to identify a reliable Pb-free material to replace the current SnPb finish for leaded components. Many suppliers have selected pure Sn since it provides good solderability and does not require major changes of the existing manufacturing infrastructure. However, the spontaneous whisker growth on Sn finish surfaces is a serious reliability issue. It is believed that the compressive stress developed in the Sn finish is the major driving force for the whisker growth, which acts as a stress relief mechanism [1]–[4]. It is also believed that the continuous increase of this stress is due to intermetallic compound formation at the Sn/lead-frame interface [3], [4]. Recently, Barsoum *et al* proposed that the compressive stress is due to the oxidation of Sn [1]. The oxygen diffuses into the grain boundaries and forms Sn oxides, which generates the compressive stress in the Sn film by increasing the volume of the confined Sn film.

The other whisker growth scenario is temperature cycling. Whiskers grow from the Sn finish on electronic packages during temperature cycling. The growth speed is much faster than the spontaneous growth during storage. The temperature cycling is often assumed to be the accelerated test of storage although the underlining physics is still under investigation.

White Sn (β -Sn) has an anisotropic body-centered tetragonal structure with its c -axis much shorter than its a -axis ($c/a = 0.546$). The elasticity anisotropy and thermal expansion anisotropy are significant [5]. So the grain orientation information, in addition to the grain size and shape of the Sn finish, should be considered when evaluating the whisker growth propensity of Sn finishes. Since stress plays a critical role in every stage of the Sn whisker growth, it is important to study the stress behavior based on the microstructure of the Sn finish and understand how the microstructure affects the stress.

However, the micromechanics problem is so complicated that one has to simplify the problem by making various assumptions. There have been some theoretical studies on the stresses in Sn, such as an analytical model based on non-equilibrium thermodynamics [4], a qualitative estimate of Young's modulus in textured Sn films [3], a finite element method (FEM) model treating Sn as an isotropic linear elastic material [2], and a 2-dimensional (2-D) FEM model treating the grains as periodic hexagonal arrangement with linear elastic material property [1]. In the present work, we will use a 3 dimensional (3-D) finite element method model to simulate columnar Sn grains on a Cu leadframe. The grain structure is explicitly established in the model by using the Voronoi Diagram method. Sn elasticity on each grain is modeled by the elastic stiffness matrix of Sn single crystal. The crystal orientations are assigned to the grains according to the information collected by X-ray diffraction (XRD). The stress along with the strain energy density distributions in grains are calculated by the FEM model for different configurations of Sn microstructure. The effect of the Sn plasticity will be explored using an a simple bilinear isotropic hardening stress-strain relation. The creep effect will not be considered in the current formulation. This work focuses on the temperature cycling test of Sn whisker growth. Although, creep is significant for Sn at high temperature, for moderate temperature rang (-55°C to 85°C) and normal loading speed (a few cycles per hour) in thermal cycling tests, the general picture is qualitatively correct without considering creep.

This work was presented on the 55th Electronic Components and Technology Conference (ECTC2005), Lake Buena Vista, Florida, USA on May 31 to June 3, 2005.

Jie-Hua Zhao, Peng Su, Min Ding and Sheila Chopin are with Freescale Semiconductor, Inc., MD:TX30/OE21, 6501 William Cannon Drive West, Austin, TX 78735.

Paul S. Ho is with University of Texas at Austin, Microelectronics Research Center, 1 University Station Stop, Mail Code R8650, Austin, TX 78712

The authors can be reached by email at: jiehuazhao@gmail.com

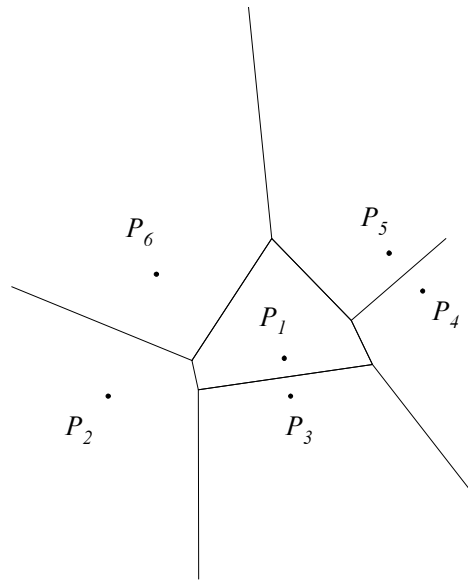


Fig. 1. A Voronoi diagram with 6 generating points. Generating point P_1 is in a Voronoi cell.

II. METHODOLOGY

A. Geometry Modeling

In order to describe the geometric characteristics of the textural Sn finish on a Cu leadframe, a Voronoi diagram method is used to generate the grain pattern. Voronoi diagrams are recently attracting the attentions of materials scientists [6]–[8]. A Voronoi tessellation can be generated in the following way. Suppose we have a finite number of distinct points, which are called the generating points, in a given space. For each generating point, draw perpendicular lines to bisect the lines joining neighboring generating points. The bisecting lines form cell walls enclosing that generating point. An example is shown in Figure 1. For generating point P_1 , five perpendicular lines are drawn to bisect the lines (not shown in the figure) connecting the neighboring points (P_2, P_3, P_4, P_5, P_6). Point P_1 is enclosed in a cell with the bisecting lines as the cell walls. The cell is called the Voronoi region or Voronoi cell. The Voronoi cells are convex polygons. This process goes on for all other points until every point is enclosed in a Voronoi region, except the edge points, which are only separated by ray lines. In Figure 1, all points are edge points except P_1 .

The Sn grains in this work are modeled as a columnar structure which can be extruded from a 2-D Voronoi diagram. The Voronoi diagram is generated using the mathematics software Mathematica [9]. The coordinates of the generating points are generated by the random number generator of Mathematica. The Voronoi diagrams are generated by calling its Computational Geometry add-on package. The average grain size is controlled by putting a proper number of generating points in a known area. The Mathematica program generates the coordinates of the vertexes of the Voronoi diagram and the connection relationship of the vertexes. To generate an FEM mesh in the finite element software ANSYS [10], an ANSYS Parametric Design Language [10] script is used to input the coordinates and connection relationship of the Voronoi diagram.

Figure 2 shows a typical grain pattern with 50 grains generated by using the Voronoi tessellation algorithm. A scanning electron microscope (SEM) picture is also shown in the figure as a comparison. The computer generated grain pattern is fairly similar to the grain pattern in the SEM picture.

B. Grain Orientation

The texture of the Sn coating is modeled by assigning a specific grain orientation to each Voronoi cell. The orientation assignment is based on the XRD data of actual samples. The texture fraction $T_f(hkl)$ for an (hkl) orientation is calculated by

$$T_f(hkl) = \frac{I(hkl)/I_0(hkl)}{\sum_{hkl}[I(hkl)/I_0(hkl)]} \quad (1)$$

where $I(hkl)$ and $I_0(hkl)$ are the intensities of (hkl) reflections measured on the textural sample and a standard β -Sn powder sample, respectively. Table I lists the texture fractions of Sn finishes deposited using two different plating baths. In that table, the 2θ is the diffraction angle. The intensities of the peaks are in arbitrary units with the maximum peak normalized to 100 for each sample itself. For powder sample, the maximum intensity peak is not listed there. The XRD results clearly show that the textures are different in these two samples.

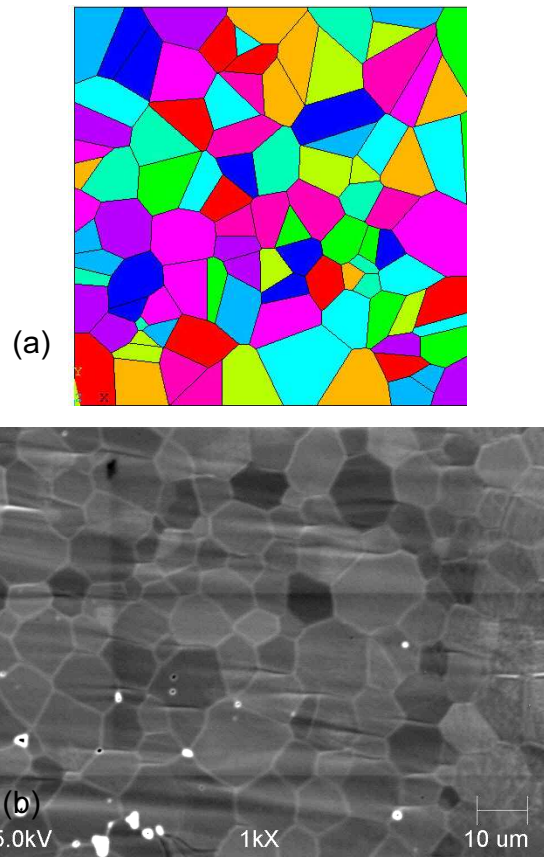


Fig. 2. (a) A typical grain pattern (Voronoi diagram) with 50 grains generated by computer using Mathematica and ANSYS. The color is arbitrarily assigned to enhance the visibility. (b) An SEM image of actual grains of the Sn finish plated on a copper leadframe.

TABLE I

X-RAY DIFFRACTION INTENSITIES AND TEXTURE FRACTIONS FOR TWO SAMPLES FROM DIFFERENT PLATING BATHS

(hkl)	$I_0(hkl)$	$2\theta(^{\circ})$	$I(hkl)$ (Bath-A)	$T_f(hkl)$ (Bath-A)	$I(hkl)$ (Bath-B)	$T_f(hkl)$ (Bath-B)
(101)	90	32.02	5.30	0.01	0.40	0
(220)	34	43.87	19.10	0.07	100.0	0.43
(211)	74	44.90	58.00	0.10	66.40	0.13
(112)	23	62.54	100.0	0.58	0.00	0
(321)	20	64.58	35.50	0.24	45.60	0.33
(420)	15	72.41	0	0	8.90	0.09
(411)	15	73.20	0	0	1.30	0.01
(312)	20	79.47	0	0	0.90	0.01

Using the the measured texture fraction $T_f(hkl)$, the previously generated cells (representing grains) of Voronoi diagram are assigned corresponding grain orientations. The XRD measurement $T_f(hkl)$ value is an integration value without specific grain information. It is not as detail as other methods, such as electron backscattering diffraction, which can index each grain. However, XRD is a fast measurement and can be incorporated in manufacturing process. The XRD data also provide great flexibility for grain assignment in the FEM modeling. It is only required to maintain the the texture fraction value of the modeled structure conforming to the measured $T_f(hkl)$ values.

Euler angles are normally used to describe the rotations of coordinates [11]. However, the definitions of Euler angles are different by different authors. The FEM software ANSYS defines Euler angles α , β and γ according to Figure 3 [10]. It consists three rotations. The first rotation is about the z -axis in the $x - y$ plane from x -axis towards y -axis to form a new coordinate system $(x_1-y_1-z_1)$ with an angle α . The second rotation is about the x_1 -axis in the y_1-z_1 plane from y_1 -axis towards z_1 -axis to form coordinate system $(x_2-y_2-z_2)$ with an angle β . The third rotation is about the y_2 -axis from z_2 -axis towards x_2 -axis to form $(x_3-y_3-z_3)$ with an angle γ [10].

The three rotation matrices of the Euler angles are defined by [11]

$$R_1(\alpha) = \begin{bmatrix} \cos(\alpha) & \sin(\alpha) & 0 \\ -\sin(\alpha) & \cos(\alpha) & 0 \\ 0 & 0 & 1 \end{bmatrix} \quad (2)$$

$$R_2(\beta) = \begin{bmatrix} 1 & 0 & 0 \\ 0 & \cos(\beta) & \sin(\beta) \\ 0 & -\sin(\beta) & \cos(\beta) \end{bmatrix} \quad (3)$$

$$R_3(\gamma) = \begin{bmatrix} \cos(\gamma) & 0 & -\sin(\gamma) \\ 0 & 1 & 0 \\ \sin(\gamma) & 0 & \cos(\gamma) \end{bmatrix} \quad (4)$$

By using the above three rotation matrices, one can rotate any vector from one direction to a given direction in a 3-D space. To assign the proper orientation to each Sn grain, the following procedure is used in the model. First, we assume every Sn grain is originally oriented with its (100) on the x -axis, (010) on the y -axis and (001) on the z -axis of the laboratory coordinates (here z -axis is the out-of-plane direction of the sample). Assume the normal of the (hkl) planes is described by the three direction cosines (a, b, c) in the lab coordinate system in this assumed “original” orientation. Then we make three rotations according to the Euler angles defined above to orient each crystal grain to get the (hkl) texture orientation. This is equivalent to rotate a vector with its direction cosines (a, b, c) to the final direction of the z -axis of the lab coordinates with direction cosines of $(0, 0, 1)$. The rotation process is expressed in terms of the rotation matrices and direction cosines in Equation (5)

$$\begin{bmatrix} 0 \\ 0 \\ 1 \end{bmatrix} = R_3(\gamma)R_2(\beta)R_1(\alpha) \begin{bmatrix} a \\ b \\ c \end{bmatrix} \quad (5)$$

Equation system (5) seems formidable. However, it can be solved after some algebra. Solving it, we have the Euler angles

$$\beta = -\arctan\left(\frac{b \cos \alpha - a \sin \alpha}{c}\right) \quad (6)$$

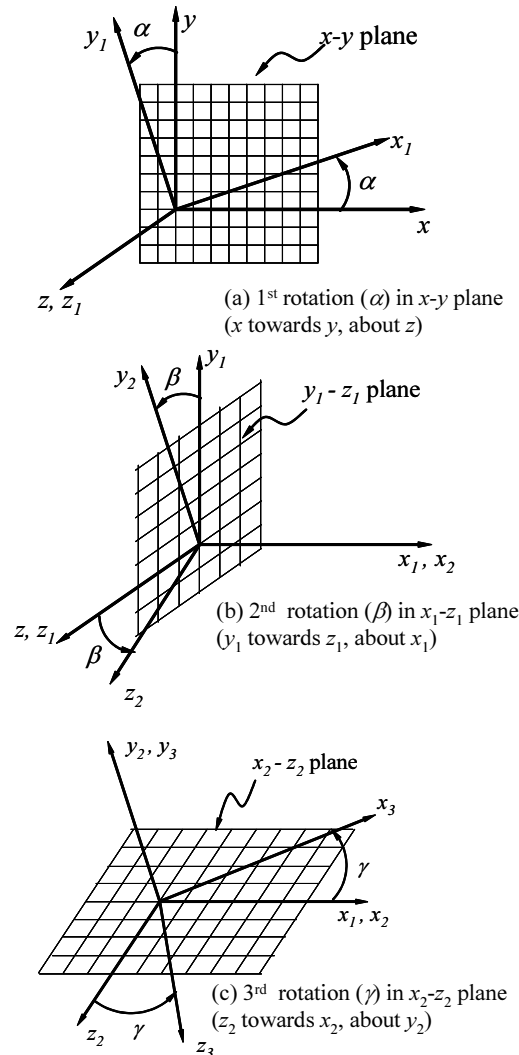


Fig. 3. Definition of Euler angles in ANSYS

$$\gamma = \arctan \left(\frac{a \cos \alpha + b \sin \alpha}{\sqrt{(b \cos \alpha - a \sin \alpha)^2 + c^2}} \right) \quad (7)$$

Where the first Euler angle α is arbitrary. It is due to an arbitrary rotation of the grain around the (hkl) axis.

In the FEM model of ANSYS, the grain orientation (hkl) is assigned to each element by rotating its element coordinate system according to the Euler angles α , β and γ determined by Equations (6) and (7).

C. Elasticity Anisotropy

β -Sn is a body-centered tetragonal crystal structure which satisfies the class $4mm$ symmetry. The generalized Hooke's law for a tetragonal single crystal with class $4mm$, $42m$, 422 or $4/mmm$ symmetry can be expressed by [12]

$$\begin{bmatrix} \sigma_{11} \\ \sigma_{22} \\ \sigma_{33} \\ \sigma_{23} \\ \sigma_{31} \\ \sigma_{12} \end{bmatrix} = \begin{bmatrix} c_{11} & c_{12} & c_{13} & & & \\ c_{12} & c_{11} & c_{13} & & & \\ c_{13} & c_{13} & c_{33} & & & \\ & & & c_{44} & & \\ & & & & c_{44} & \\ & & & & & c_{66} \end{bmatrix} \begin{bmatrix} \varepsilon_{11} \\ \varepsilon_{22} \\ \varepsilon_{33} \\ \varepsilon_{23} \\ \varepsilon_{31} \\ \varepsilon_{12} \end{bmatrix} \quad (8)$$

The elastic stiffness matrix elements (in GPa) of β -Sn near the room temperature are $c_{11} = 109.4$, $c_{33} = 107.8$, $c_{12} = 57.67$, $c_{13} = 34.76$, $c_{66} = 26.75$, and $c_{44} = 2.56$ [5].

The elastic stress-strain relation of an orthotropic material is expressed in Equation (9) [10].

$$\begin{bmatrix} \varepsilon_{xx} \\ \varepsilon_{yy} \\ \varepsilon_{zz} \\ \gamma_{xy} \\ \gamma_{xz} \\ \gamma_{yz} \end{bmatrix} = \begin{bmatrix} \frac{1}{E_x} & \frac{-\nu_{xy}}{E_y} & \frac{-\nu_{xz}}{E_z} \\ \frac{-\nu_{yx}}{E_x} & \frac{1}{E_y} & \frac{-\nu_{yz}}{E_z} \\ \frac{-\nu_{zx}}{E_x} & \frac{-\nu_{zy}}{E_y} & \frac{1}{E_z} \\ & & & \frac{1}{G_{xy}} \\ & & & & \frac{1}{G_{yz}} \\ & & & & & \frac{1}{G_{xz}} \end{bmatrix} \begin{bmatrix} \sigma_{xx} \\ \sigma_{yy} \\ \sigma_{zz} \\ \sigma_{xy} \\ \sigma_{xz} \\ \sigma_{yz} \end{bmatrix} \quad (9)$$

with the constraints

$$\frac{\nu_{yx}}{E_x} = \frac{\nu_{xy}}{E_y}, \quad \frac{\nu_{zx}}{E_x} = \frac{\nu_{xz}}{E_z}, \quad \frac{\nu_{zy}}{E_y} = \frac{\nu_{yz}}{E_z} \quad (10)$$

The elastic compliance matrix S (with elements s_{ij}) is the inverse of C (with elements c_{ij}):

$$S = C^{-1} = \begin{bmatrix} s_{11} & s_{12} & s_{13} & & & \\ s_{12} & s_{11} & s_{13} & & & \\ s_{13} & s_{13} & s_{33} & & & \\ & & & s_{44} & & \\ & & & & s_{44} & \\ & & & & & s_{66} \end{bmatrix} \quad (11)$$

The conversion from elastic compliance matrix elements to the engineering constants (E_x , ν_{xy} and so on) is the following [13]

$$\begin{aligned} E_x = E_y = 1/s_{11}, \quad E_z = 1/s_{33}, \\ G_{xy} = G_{yz} = 1/s_{44}, \quad G_{xz} = 1/s_{66}, \\ \nu_{xz} = \nu_{yz} = -s_{13}/s_{33}, \quad \nu_{xy} = -s_{12}/s_{11} \end{aligned} \quad (12)$$

Therefore, the elastic behavior of β -Sn single crystal can be described by the engineering constants with $E_x = E_y = 76.20\text{GPa}$, $E_z = 93.33\text{GPa}$, $G_{xy} = 26.75\text{GPa}$, $G_{yz} = G_{xz} = 2.56\text{GPa}$, $\nu_{xy} = 0.473$, $\nu_{xz} = 0.170$ and $\nu_{yz} = 0.208$. The coefficient of thermal expansion is $\alpha_x = \alpha_y = 15.8 \times 10^{-6}/^\circ\text{C}$, and $\alpha_z = 28.4 \times 10^{-6}/^\circ\text{C}$ [5].

D. Plasticity Effect

A good treatment of Sn grain plasticity should follow the crystal plasticity theory [14], [15]. However, this theory makes additional assumptions on slip system resistance parameters. An experimental calibration of its constitutive parameters is needed before the crystal plasticity model can be used. Unfortunately, there is no β -Sn crystal plasticity model existing at present time.

Isotropic hardening is normally a good approximation of low melting point poly-crystalline metals such as Sn [16]. In this study, a bilinear isotropic hardening rule is used to approximate the plastic behavior of Sn. This approximation does not consider the crystal orientations and slip systems, which may not be realistic. However, due to the lack of material property data and no better existing plastic model, we will use this as a first order approximation in this work. According to Diulin *et*

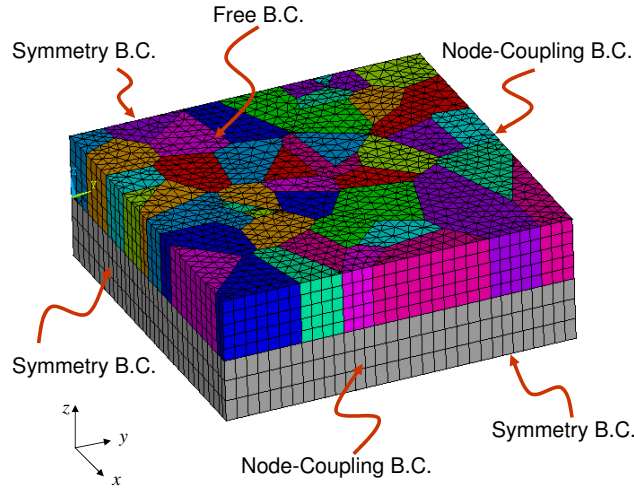


Fig. 4. A typical FEM mesh with boundary conditions. Sn grains with different grain orientations are color-coded. The Cu leadframe is modeled as an isotropic material.

al [17], single crystal β -Sn (with 0.01 to 0.53 atomic% Zn) yields at 9.2 MPa (uniaxial tension) at room temperature and the tangent modulus is 85 MPa in the bilinear isotropic hardening model. These data were measured on single crystal Sn samples with proper axis of elongation such that the maximum shear stress was attained in the slip system $(100)\langle 010 \rangle$. These two parameters will be used to account for the plastic behavior of β -Sn on copper leadframes.

E. Strain Energy Density

Although compressive stress is believed to be the driving force of Sn whisker growth [1]–[4], its tensorial nature makes the stress hard to serve as a one-parameter criterion for whisker growth. However, if energy based criterion is used, it is possible to use one parameter to describe the risk of whisker growth. We choose strain energy density (SED) as the parameter to describe the whisker growth propensity. Strain energy density is defined by

$$w = \int \sigma_{ij} d\varepsilon_{ij} \quad (13)$$

Here summation of repeated indices is assumed. In this definition, elastic and inelastic strain energy density are included. SED actually combines both stress and strain effect.

Strain energy density has an unit of Joule/m³(=Pascal). MPa will be used as the SED unit in this work. In the ANSYS calculation, an element table manipulation is used to generate the SED in the post processing stage. The goal of this study is to determine if there is a correlation of calculated SED and the experimentally measured Sn whisker growth propensity.

F. Finite Element Model

The finite element model is implemented by using the commercial software ANSYS. ANSYS provides an anisotropic element called Solid64 which can account for the elastic anisotropy by taking the full elastic stiffness matrix as its input. However, this element does not support plasticity. Since the tetragonal structure of β -Sn falls in the category of orthotropic materials. We can take the advantage of the regular continuous solid elements of ANSYS such as Solid45 and Solid185. The 3-D 8-node solid element Solid185 is used here. This element has large deformation capability and supports orthotropic elasticity and plasticity. It is also proven that the convergence performance is better than other elements, such as Solid45.

The Mathematica generated Voronoi diagram grain pattern is read into ANSYS. A columnar Sn grain structure is assumed. An extrusion of the Voronoi diagram forms a 3-dimensional mesh. For thin Sn films, say about 10 μ m, columnar grain pattern is a very good assumption although at some portion, there are occasionally some stacking grains in the film thickness direction. Sn is modeled with the elasto-plastic model described above. Cu leadframe is modeled as a linear elastic material with Young's modulus of 117GPa, Poisson's ratio of 0.345 and CTE of 17ppm/ $^{\circ}$ C.

A $56\mu\text{m} \times 56\mu\text{m}$ square of the Sn-coated Cu leadframe is modeled. 50 Sn grains with average grain size of about $8\mu\text{m}$ is considered. The symmetry boundary condition is applied to a leadframe surface to simulate the fact that the leadframe has two-sided Sn finish. The Sn finish surface is modeled with the free boundary. The other 4 sides of the 3-D models are modeled with two sides (left and bottom in Figure 4) of symmetry boundary conditions and the other two sides (right and top in Figure 4) of node-coupling boundary condition. A corner node is fixed to eliminate the rigid body motion.

Since the intrinsic compressive stress is normally observed in Sn film on Cu [1]–[4], the intrinsic stress is assumed in the FEM model. Following Lau and Pan [2], 8MPa compressive stress at 20 $^{\circ}$ C is applied to Sn by calling the ANSYS

TABLE II
WHISKER PROPENSITY OF Sn ON Cu LEADS

Plating Bath	Whiskers per lead	Maximum length (μm)
A	4	15
B	35	65

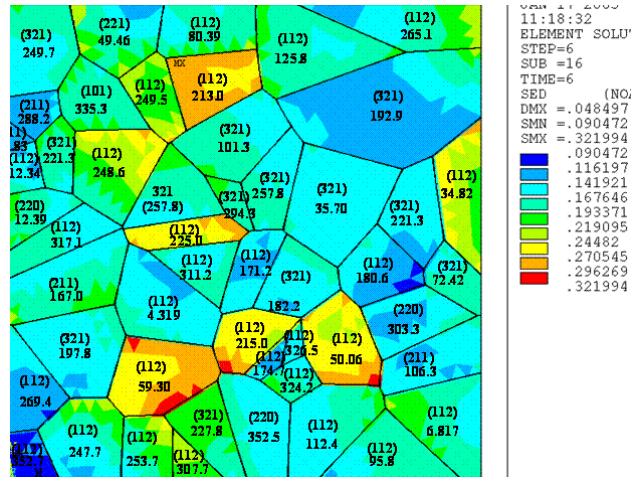


Fig. 5. Strain energy density of Sn film deposited using Bath-A. The grain orientation of each grain is identified by a texture orientation (hkl) followed by an in-plane rotation angle (α in Equation 5 and Figure 3) starting from the x-axis of the lab coordinates.

initial stress command ISTRESS. This stress is applied as a hydrostatic pressure, i.e., $\sigma_{xx} = \sigma_{yy} = \sigma_{zz} = -8$ MPa and $\tau_{xy} = \tau_{yz} = \tau_{zx} = 0$. This is an approximation and is purely for simplicity reason. The initial stress of an element is only applied at time zero and the original value will not sustain if there is no confinement to that element. In the out-of-plane direction, there is no external constraint after time zero. The hydrostatic pressure kind of initial stress will become an "in-plane bi-axial stress" in the Sn film after time zero since the Cu leadframe is the only external confinement to the Sn film. This ANSYS trick helps us to simplify the process of resolving the in-plane initial stress in each local elemental coordinate system for each crystal grain, which has different orientation. However, strictly speaking, the intrinsic compressive stress applied in the FEM model of Sn film may be different than 8MPa due to the Poisson effect.

Thermal loads were studied to mimic the air-to-air temperature cycling test. 6 loading steps were applied: 20°C to -55°C (Step 1), -55°C to 85°C (Step 2), 85°C to -55°C (Step 3), -55°C to 85°C (Step 4), 85°C to -55°C (Step 5), and -55°C to 85°C (Step 6).

III. RESULTS

Two different plating samples were studied. The Sn finishes of the two leadframes were plated in different baths. The XRD results are tabulated in Table I. The corresponding grain structures were generated to conform the textural fraction of Table I.

Table II lists the test results of samples from the two different baths. The test was a temperature cycling accelerated test. The whisker counts and length measurements were done after 1000 cycles of -55°C to 85°C air-to-air temperature cycling. For Bath-A, the average whisker numbers on each lead of the package is 4 with a maximum whisker length of 15 μm . For Bath-B, the corresponding values are 35 whiskers per lead and a 65 μm maximum whisker length. It will be shown that the calculated volume distribution of SED has a correlation to the whisker propensity. The higher SED value corresponds to higher Sn whisker count and length.

Figures 5 and 6 are the contour plots of the calculated strain energy density of the two samples after 6 consecutive temperature load steps. In these figures, the grain patterns overlay the corresponding SED contours. Each grain is indexed by its texture orientation (hkl) followed by an in-plane rotation angle (α in Equation 5 and Figure 3) starting from the x-axis of the lab coordinates. The rotation procedure is described in the previous subsection by Equation (5). The plasticity is considered by using the isotropic bilinear hardening rule described above. In Figures 5 and 6, some grains have a high SED and others have a low SED. The maximum SED in Figure 6, which corresponds to Bath-B, is 0.371 MPa. The corresponding value for Bath-A in Figure 5 is 0.322MPa. It is also clear that the high SED portion is located in some grains with specific orientations. In Figure 5 high SED is in (112) grains. In Figure 6, the high SED is in (220) grains and a (420) grain. This phenomenon is an indication of anisotropy of elasticity and thermal expansion. However, due to the random in-plane rotation (α), not every grain with the same (hkl) is in the worst position to suffer the high SED. An example of Young's modulus spacial distribution

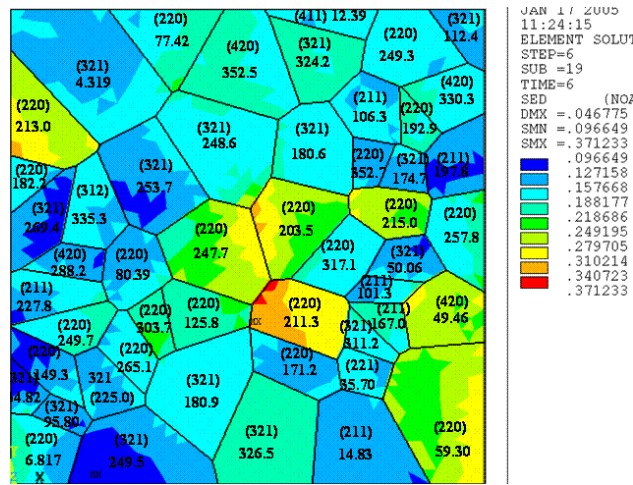


Fig. 6. Strain energy density of Sn film deposited using Bath-B. The grain orientation of each grain is identified by a texture orientation (hkl) followed by an in-plane rotation angle (α in Equation 5 and Figure 3) starting from the x-axis of the lab coordinates.

around the angle α is studied in [3]. Another important phenomenon we observed from these figures is that the highest SED is always near the grain boundaries. This explains the fact that Sn whiskers are normally observed at the boundaries of grains experimentally as shown in Figure 9.

If we assume that the Sn whisker growth tendency is proportional to the SED and the area under high SED, then a statistical analysis of the calculated SED of both Bath-A and Bath-B may give us more information. Figure 7 plots the volume distribution of the SED for both Bath-A and Bath-B. The horizontal axis of Figure 7 is the SED. The vertical axis represents the volume fraction with the SED higher or equal to the value of the horizontal coordinate value. For example, in case an SED value on the horizontal axis is 0.3MPa, on the curve “Plating Bath A” of the lower panel about 3×10^{-3} (or 0.3%) of the volume of the Sn coating plated in Bath-A has an SED higher than or equal to 0.3 MPa. Corresponding to the curve “Plating Bath B”, about 2×10^{-2} (or 2%) of the Sn has an SED higher than or equal to 0.3MPa. From Figure 7, we can clearly see that the Sn finish produced by Bath-B consistently has more volume of Sn material under higher SED than that of Bath-A. From the statistic data of Figure 7, it is confident to believe that the sample with Bath-A will perform better than the sample with Bath-B in the Sn whisker accelerated tests provided the assumption that higher SED promotes whisker growth holds. This is clearly proven by the experimental data listed in Table II.

The upper panel of Figure 7 shows the time evolution of the SED of Sn coating from Bath-A and Bath-B. As the temperature cycling progresses, the SED keeps increasing statistically, i.e., more and more volume of Sn is under higher SED. This means that the SED accumulates when temperature cycling progresses. The SED accumulation is a direct manifestation of the Sn plasticity. The SED accumulation explains why we see Sn whiskers grow after a certain number of temperature cycles. Although the plasticity model used here is only a first order approximation, it does explain some of the experimental facts. It is evident that Bath-B consistently has larger fraction of volume under high SED than that of Bath-A at each loading step of the first 6 steps. This gap has a tendency of getting larger and larger as temperature cycling progresses. This has a direct correlation with the experimental data in Table II.

If the model only considers the elasticity, SED will be the same as temperature cycling progresses. Figure 8 shows the calculated SED results without considering Sn plasticity. The anisotropy of elasticity does considered in the calculation. The thermal loads are from 20°C to -55°C (Step 1) and from 20°C to 85°C (Step 2). More fraction of volume is under higher SED for Bath-B than that of Bath-A at both temperatures. This is also a good correlation with the experimental data in Table II.

Since the compressive stress is believed to be the driving force of the whisker formation in Sn finish, we may postulate that the hydrostatic stress is responsible for Sn whisker growth. The hydrostatic stress is defined by $(\sigma_1 + \sigma_2 + \sigma_3)/3$, where σ_1 , σ_2 , and σ_3 are the three principal stresses. Figure 10 plots the hydrostatic stress $(\sigma_1 + \sigma_2 + \sigma_3)/3$ distribution when Sn plasticity is not considered. Since yielding are not considered and only pure elastic behavior of Sn is considered, the compressive stress is so large that some area is more than 150MPa. If we assume that the whiskering is the primary stress relieving mechanism, then this kind of plot has its practical meaning. The higher the compressive hydrostatic stress (with a negative sign but larger absolute value) the higher the risk of Sn whisker growth. The elastic response will no change as the temperature cycling progress. Two distributions (at -55°C and at 85°C), represent the two possible stress distributions. It is clearly shown that, at high temperature end of the thermal cycle (85°C), the two baths show very similar stress behavior. However, at the low temperature end of the thermal cycle -55°C, more volume fraction of Sn is under higher compressive stress for the Bath-B sample than that of the Bath-A sample. This also agrees well with the test results of Table II, which says that Sn finish produced by Bath-B is more prone to whisker growth.

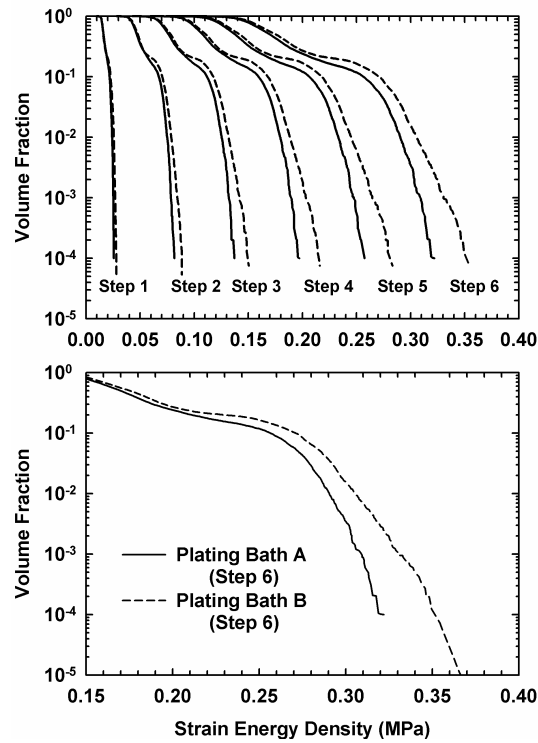


Fig. 7. Strain energy density distribution comparison for Bath-A and Bath-B. The upper panel is the SED distribution in the first 6 temperature load steps. The lower panel shows the detail of load step 6. The horizontal axis is the SED. The vertical axis represents the volume fraction with the SED higher than or equal to the value of the horizontal coordinate value. The solid lines represent Bath-A and the dashed lines represent Bath-B. More fraction of volume is under higher SED for Bath-B than that of Bath-A for each load step.

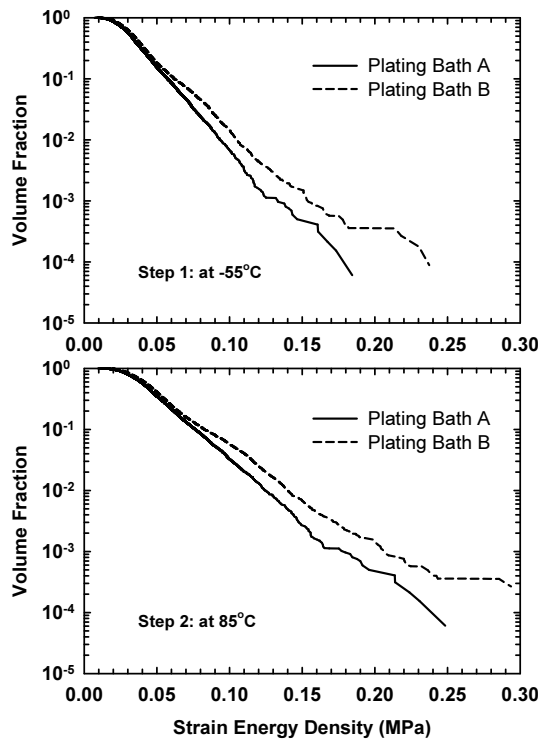
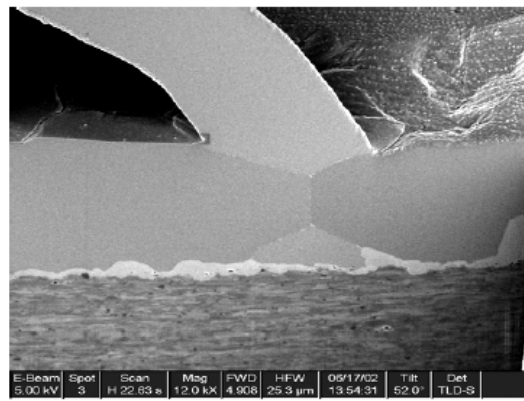
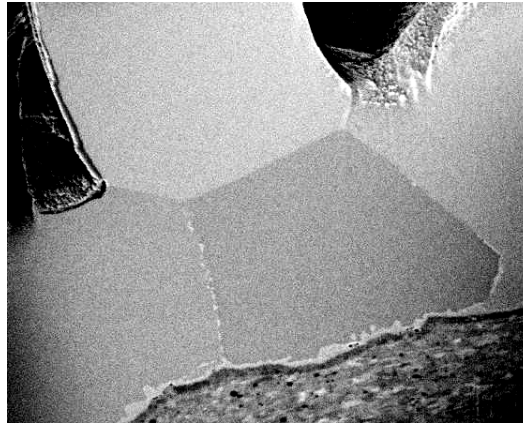


Fig. 8. Strain energy density distribution when plasticity is not considered. The solid lines are for Bath-A and the dashed lines are for Bath-B. The thermal loads are from 20°C to -55°C (Step 1) and from 20°C to 85°C (Step 2). More fraction of volume is under higher SED for Bath-B than that of Bath-A at both temperatures.



(a)



(b)

Fig. 9. Examples of Sn whiskers growing on top of grain boundaries. (a) a whisker growing on top of the grain boundary of two Sn grains, (b) a whisker growing on top of two grain boundaries of three Sn grains

It should be mentioned that we have fully considered the elasticity and thermal expansion anisotropy, but not considered the deemed plasticity anisotropy. We simply borrowed the polycrystal plasticity constitutive law to account for the single crystal plasticity, which is the limitation of the current model. As we mentioned before, the crystal plasticity theory, which accounts for the effect of slip systems in single crystals, may be the path to breakthrough this limitation. Nevertheless, the SED is insensitive to the exact form of the plasticity constitutive law, which has been proven by the good correlation of the experimental results in Table II and the simulation results in Figure 7. The simplified plasticity model presented here is useful if the SED criterion is adapted for Sn whisker growth.

The creep effect is not considered in the current study. It will be very interesting to see how the creep affects the results. The future work will be considering the crystal plasticity and creep of Sn. With the crystal plasticity considered, the anisotropy effect of Sn grain is fully accounted. With these mentioned improvements, the current model can be extended to a full-fledged microstructural model for Sn whisker growth prediction. However, even with its current form, if the strain energy density criterion is taken as the Sn whisker growth driving force, the model is validated by experiments and can be used to study the whicker growth tendency. The stress-based criterion is more sensitive to the exact form of the plasticity constitutive law. If only anisotropy of elasticity and thermal expansion is considered, using the relative comparison of the stress distributions to predict the whisker growth tendency is also attested by the experimental results.

IV. CONCLUSIONS

A 3-D FEM model considering the elasticity anisotropy, thermal expansion anisotropy and plasticity of β -Sn is established. The model makes use of the Voronoi diagram algorithm to generate the geometry of Sn grains on Cu leadframes. The crystal orientations are assigned to the Sn grains in the model using the x-ray diffraction measurement data of actual samples. The model is applied to the Sn-plated package leads under thermal cycling tests. The strain energy density is calculated for each grain. The modeling results are compared with the whisker growth data. A preliminary correlation of the simulation results is established with the whisker growth propensity. These results suggest that the finite element modeling has the potential to

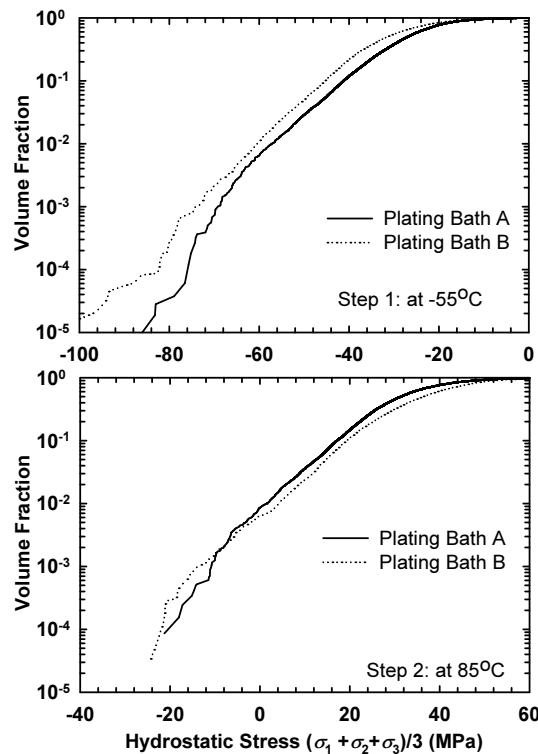


Fig. 10. The hydrostatic stress $(\sigma_1 + \sigma_2 + \sigma_3)/3$ distribution at two temperatures when the Sn plasticity is not considered. The vertical axis represents the volume fraction with the hydrostatic stress lower than or equal to the value of the horizontal coordinate. The solid lines are for Bath-A and the dashed lines are for Bath-B.

predict the whisker growth propensity and provides directions on establishing an analytical model for Sn whisker growth. The limitation and possible improvement of the current model are also discussed.

V. ACKNOWLEDGMENTS

The whisker propensity measurement done by Jim Howell is greatly appreciated. JHZ would also like to thank Trent Uehling and Dave Wontor for management support of this work.

REFERENCES

- [1] M. W. Barsoum, E. N. Hoffman, R. D. Doherty, S. Gupta, and A. Zavalaingos, "Driving force and mechanism for spontaneous metal whisker formation," *Physical Review Letters*, vol. 93, art. 206104, 2004.
- [2] J. H. Lau and S. H. Pan, "3D nonlinear stress analysis of tin whisker initiation on lead-free components," *Transactions of ASME Journal of Electronic Packaging*, vol. 125, pp. 621–624, December 2003.
- [3] B.-Z. Lee and D. N. Lee, "Spontaneous growth mechanism of tin whiskers," *Acta Materialia*, vol. 46, no. 10, pp. 3701–3714, 1998.
- [4] K. N. Tu, "Irreversible process of spontaneous whisker growth in bimetallic Cu-Sn thin-film reactions," *Physical Review B*, vol. 49, no. 3, pp. 2030–2034, 1994.
- [5] R. Ravelo and M. Baskes, "Equilibrium and thermodynamic properties of grey, white, and liquid tin," *Physical Review Letters*, vol. 79, no. 13, pp. 2482–2485, 1997.
- [6] B. de Lacy Costello and N. Ratcliffe, "The formation of Voronoi diagrams in chemical and physical systems: experimental findings and theoretical models," *International Journal of Bifurcation and Chaos*, vol. 14, no. 7, pp. 2187–2210, 2004.
- [7] D.-S. Kim, Y.-C. Chung, J. J. Kim, D. Kim, and K. Yu, "Voronoi diagram as an analysis tool for spatial properties for ceramics," *Journal of Ceramic Processing Research*, vol. 3, no. 3, pp. 150–152, 2002.
- [8] V. R. Vedula, S. J. Glass, D. M. Sayl, G. S. Rohrer, W. C. Carter, S. A. Langer, and E. R. Fuller Jr., "Residual-stress predictions in polycrystalline alumina," *Journal of American Ceramic Society*, vol. 84, no. 12, pp. 2947–2954, 2001.
- [9] *Mathematica 5.1*, Wolfram Research, 2004. [Online]. Available: <http://www.wolfram.com>
- [10] *ANSYS 8.1*, ANSYS Inc., 2004. [Online]. Available: <http://www.ansys.com>
- [11] G. B. Arfken and H. J. Weber, *Mathematical Methods for Physicists*, 4th ed. Academic Press, 1995.
- [12] J. F. Nye, *Physical Properties of Crystals*. Oxford: Clarendon Press, 1960.
- [13] S. G. Lekhnitskii, *Theory of Elasticity of an Anisotropic Elastic Body*. San Francisco: Holden-Day, 1963.
- [14] L. Anand, "Single-crystal elasto-viscoplasticity: application to texture evolution in polycrystalline metals at large strains," *Computer Methods in Applied Mechanics and Engineering*, vol. 193, pp. 5359–5383, 2004.
- [15] L. Anand and M. Kothari, "A computational procedure for rate independent crystal plasticity," *Journal of the Mechanics and Physics of Solids*, vol. 44, no. 4, pp. 525–558, 1996.
- [16] J. Lubliner, *Plasticity Theory*. New York: Collier Macmillan, 1990.
- [17] A. N. Diulin, G. I. Kirichenko, V. D. Natsik, and V. P. Soldatov, "Low-temperature plasticity of Zn-doped β -Sn crystal," *Low Temperature Physics*, vol. 23, no. 10, pp. 843–847, 1997.

Jie-Hua Zhao (M01) received the B.S. and M.S. degrees in physics from Tsinghua University, Beijing, China, in 1989 and 1991, respectively, and the Ph.D. degree from the Department of Physics, University of Texas at Austin, in 2000. He is currently a packaging engineer with Texas Instruments Incorporated, Dallas, Texas. Before joining TI in 2005, he had been a Senior Staff Scientist/Principal Staff Scientist with Motorola/Freescale for five years. He was a Junior Faculty Member with Tsinghua University, Beijing, China, from 1991 to 1994. His research has included electronic structures of quantum well systems, low-k thin film characterization, package deformation characterization, moire interferometry, interfacial fracture mechanics, low-k chip-package interaction, Sn whisker growth, package stress modeling, and electromigration modeling. Dr. Zhao received the Best Paper Award for the Mechanics Track of IThERM04 Conference. He was a Session Chair at the IThERM04 and IThERM'06 Conference.

Peng Su received the Ph.D. degree in the field of material science and engineering from Cornell University in 2000. Previously he received the B.E. and M.E. degrees from Tsinghua University, Beijing, both in the field of Materials Science and Engineering. He is currently a senior packaging technologist with Freescale Semiconductor's Technology Solutions Organization. His recent research and development efforts have included the growth mechanism and mitigation strategies of whisker growth on Pb-free lead finishes, as well as material and structural innovations for thermally enhanced ball grid array packages. Previously he was with Motorola's Semiconductor Products Sector's wafer manufacturing division and was responsible for the yield improvement of MEMS sensor devices. He has co-authored over 40 conference and peer-reviewed journal papers on various packaging related subjects, and is an active member of iNEMI's Sn Whisker Test Method Standardization committee.

Min Ding has been with Freescale Semiconductor (formerly Motorola's Semiconductor Products Sector) since 2005. His current research interests are in the reliability of the BGA solder joints on component and board level. Min Ding received his M.S. (2000) in material science and engineering from the Tsinghua University, Beijing, China.

Sheila Chopin received the B.S. degree in mechanical engineering from Southern University, Baton Rouge, Louisiana in 1984 and the MBA degree from University of Phoenix in 2001. She is the manager of the Material Technology Integration group with Freescale's Technology Solutions Organization. The research and development efforts of this group provides fundamental understanding of packaging materials' thermal, mechanical, and electrical behaviors, as well as innovative and robust packaging solutions for a wide variety of package families. She has been with Freescale Semiconductor / Motorola's Semiconductor Products Sector for 13 year. Previously she was with Texas Instrument for 5 years, responsible for the development of assembly processes for various packages.

Paul S. Ho (M91SM93F02) is the Director of the Laboratory for Interconnect and Packaging at The University of Texas at Austin. He received his B.S. degree in mechanical engineering from National Chengkung University, Taiwan; M.S. degree in physics from National Tsinghua University, Taiwan; and Ph.D. degree in physics from Rensselaer Polytechnic Institute. He joined the Materials Science and Engineering Department at Cornell University in 1966 and became an Associate Professor in 1972. In 1972, he joined the IBM T.J. Watson Research Center and has held a number of management positions. In 1985, he became Senior Manager of the Interface Science Department. In 1991, he joined the faculty at The University of Texas at Austin and was appointed the Cockrell Family Regents Chair in Materials Science and Engineering. His current research is in the areas of materials and processing science for interconnect and packaging for microelectronics. He holds the inventorship of 11 U.S. Patents in microelectronics technology. He has edited six books and published extensively in the area of thin films and materials science for microelectronics. He is a Fellow of the American Physical Society, the American Vacuum Society and IEEE.